

A numerical method to compute optical conductivity based on the pump-probe simulations

Can Shao,¹ Takami Tohyama,² Hong-Gang Luo,^{1,3} and Hantao Lu^{1,*}

¹*Center for Interdisciplinary Studies & Key Laboratory for Magnetism and Magnetic Materials of the MoE, Lanzhou University, Lanzhou 730000, China*

²*Department of Applied Physics, Tokyo University of Science, Tokyo 125-8585, Japan*

³*Beijing Computational Science Research Center, Beijing 100084, China*

(Dated: March 11, 2019)

A numerical method to calculate optical conductivity based on a pump-probe setup is presented. Its validity and limits are tested and demonstrated via the concrete numerical simulations on the half-filled one-dimensional extended Hubbard model both in equilibrium and out of equilibrium. By employing either a step- or a Gaussian-like probing vector potential, it is found that in nonequilibrium, the method in the narrow-probe-pulse limit can be identified with variant types of linear response theory, which, in equilibrium, produce identical results. The observation reveals the underlying probe-pulse dependence of the optical conductivity calculations in nonequilibrium, which may have its applications in the theoretical analysis of ultrafast spectroscopy measurements.

PACS numbers: 71.27.+a, 78.47.-p

I. INTRODUCTION

Time-resolved spectroscopy has been extensively employed to investigate the dynamic properties of materials with strong correlations, e.g., the (quasi)one-dimensional (1D) Mott insulators such as bis(ethylendithyo)-tetrathiafulvalene-difluorotetracyanoquinodimethane ET-F₂TCNQ^{1–3} and the halogen-bridged transition-metal compounds^{4,5}, and the correlated systems with higher space dimensions, such as cuprates^{6–9} and manganites^{10,11}. As a promising time-resolved spectroscopy technique, the ultrafast pump-probe optical measurement is able to unravel the complicated entanglement of various degrees of freedom in a correlated system to some extend by resolving their contributions separately at multiple time scales¹². For experiments on electronic systems, the time-resolved optical conductivity is an essential quantity, from which the dynamic properties of charges and other related degrees of freedom can be analyzed, e.g., see the discussions in Refs. 13 and 14.

Generally, in order to calculate a dynamic response function of a system, related correlation functions at different moments should be obtained. The task becomes more demanding in nonequilibrium due to the absence of time-translation invariance: the correlation functions with two time variables, in general, cannot be reduced to functions with only one time variable, usually the temporal distance if the time-translation invariance holds. Theoretically, there can be various ways to investigate the nonequilibrium dynamic response of correlated systems in model calculations. One possible way is based on the nonequilibrium Green’s functions, where by using the Kadanoff-Baym or Keldysh formalism, methods which have been applied to correlated systems in equilibrium, such as the dynamic mean-field theory, can be adapted to nonequilibrium on a formal level (see, e.g., Ref. 15 and references there). Another way starts from

wave functions, which is primarily employed to closed systems. The time-dependent wave functions can be secured by various numerical methods, such as the exact diagonalization and the density-matrix renormalization group. Thereafter the expectation values of observables as functions of time, and various temporal correlations can be readily obtained, which enables further calculations on the out-of-equilibrium dynamic response. Specifically, when the time-dependent optical conductivity is concerned, several related yet different schemes, including the nonequilibrium generalizations of the Kubo formula¹⁶, linear response theory^{17,18}, or a direct calculation on dynamic current-current correlations for transient states¹⁹, have been employed on quite similar models. Naturally, the issue of the underlying characters and the validity of these approaches can be raised, which, in our opinion, has not yet been fully addressed. It is also a practical problem for the purpose of analyzing data from (sub)THz spectroscopy measurements, where the temporal resolution has been pushed up to the order of a few ten femtoseconds⁹.

In this paper, we suggest that the manners of how the temporal correlations are incorporated can be crucial in the study of nonequilibrium dynamics. Inspired by the pump-probe setup in the experiments, we propose a method to calculate the optical conductivity. Its validity and limits are demonstrated by the detailed numerical simulations on the 1D half-filled extended Hubbard model, a prototype of strongly correlated electronic systems. A comparison study between our method and the existing ones shows that by adopting two different limits on the probe pulse, our method can reproduce the results of two types of linear response theory respectively. In some nonequilibrium situations, the two sets of results on the time-dependent optical conductivity can be quite different. The theoretical analysis combined with numerical simulations elucidates the difference and connections between these various methods to a satisfactory level.

It also raises the issue of the probe-pulse dependence in nonequilibrium analysis, which has been largely ignored in previous studies.

The rest of the paper is organized as follows. In Sec. II, after the model description and a critical review on the relevant existing methods, our approach is presented. The following section provides a theoretical analysis on the validity of the approach, with numerical demonstrations concerning the options for probe-pulse parameters. In Sec. IV, comprehensive comparisons and analysis are made. The conclusion is drawn in Sec. V.

II. MODEL AND METHODS

The Hamiltonian we use in the discussion is the well-known 1D extended Hubbard model at half-filling:

$$\begin{aligned} H = & -t_h \sum_{i,\sigma} \left(c_{i,\sigma}^\dagger c_{i+1,\sigma} + \text{H.c.} \right) \\ & + U \sum_i \left(n_{i,\uparrow} - \frac{1}{2} \right) \left(n_{i,\downarrow} - \frac{1}{2} \right) \\ & + V \sum_i (n_i - 1) (n_{i+1} - 1), \end{aligned} \quad (1)$$

where $c_{i,\sigma}^\dagger$ ($c_{i,\sigma}$) is creation (annihilation) operator of electron with spin σ at site i , $n_{i,\sigma} = c_{i,\sigma}^\dagger c_{i,\sigma}$, $n_i = n_{i,\uparrow} + n_{i,\downarrow}$, t_h is the hopping constant, U and V are on-site and nearest-neighbor Coulomb repulsion interactions, respectively. In the following, we set t_h and t_h^{-1} as energy and time units and take Plank constant $\hbar = 1$, and the elementary charge $e = 1$.

We also restrict our discussions to zero temperature since the results there are most transparent. Before going to our method in detail, we first present some existing methods which are relevant to our discussions.

It is well known that the optical conductivity in equilibrium can be calculated by the Kubo formula (KF) in the linear response regime. The regular part of the optical conductivity (excluding the possible singularity at $\omega = 0$) in general is given by the current-current correlation function as:

$$\begin{aligned} \text{Re } \sigma_{\text{reg}}(\omega) &= -\frac{1}{\omega L} \lim_{\eta \rightarrow 0+} \text{Im } \chi(\omega + i\eta) \\ &= \frac{\pi}{L} \sum_{n \neq 0} \frac{1}{E_{n0}} |\langle 0 | j | n \rangle|^2 [\delta(\omega - E_{n0}) + \delta(\omega + E_{n0})], \end{aligned} \quad (2)$$

where the electric susceptibility $\chi(\omega)$ is calculated by

$$\chi(\omega) = \int_{-\infty}^{+\infty} e^{i\omega s} (-i)\theta(s) \langle 0 | [j(s), j(0)] | 0 \rangle \, ds, \quad (3)$$

and $E_{n0} := E_n - E_0$, L is the lattice size. $j(t)$ in Eq. (3) is the Heisenberg representation of the current operator j , which reads

$$j = -it_h \sum [c_{i,\sigma}^\dagger c_{i+1,\sigma} - \text{H.c.}] \quad (4)$$

In nonequilibrium, on the other hand, when the time translation invariance does not hold in general, a full two-time *response function* is required in order to describe the linear response of the electrical current with respect to a time-dependent probing field $\delta\mathbf{E}(t)$ ^{20,21}:

$$\delta\langle \mathbf{j}(t') \rangle = \int_{-\infty}^{t'} \sigma(t', t) \delta\mathbf{E}(t) \, dt. \quad (5)$$

According to the definition, the response function $\sigma(t', t)$ measures the current response at the moment t' with respect to a perturbation of an *unit pulse* at the moment t ²². After the response function is determined, for any given perturbation field $\delta\mathbf{E}(t)$, the induced current, in the linear response regime, can be calculated accordingly by Eq. (5). However for another related and important quantity, the time-dependent *optical conductivity* which we will mainly focus on, there is no unique definition if the time-translation invariance does not hold in the response function^{18,20}. Here we make it clear that the optical conductivity is the measure of the response of the system in the *frequency space* with respect to a perturbation. Following Ref. 18, throughout the article we define the conductivity to be:

$$\sigma(\omega, t) = \int_0^{t_m} \sigma(t+s, t) e^{i(\omega+i\eta)s} \, ds, \quad (6)$$

where we have explicitly introduced a spectral broadening factor η and the window width t_m for the Fourier transformations which will be used in the numerical simulations. In practice t_m is the maximum of probe duration time, which in THz spectroscopy is usually several hundred times larger than the microscopic time unit (e.g., t_h^{-1} here).

In the linear response regime, rigorous analysis produces the response function $\sigma(t', t)$ as (with restriction $t' \geq t$)^{17,18}

$$\sigma(t', t) = \frac{1}{L} \left[\langle \psi(t') | \tau | \psi(t') \rangle + \int_t^{t'} \chi(t', t'') \, dt'' \right], \quad (7)$$

where the two-time susceptibility is

$$\chi(t', t'') = -i\theta(t' - t'') \langle \psi(t) | [j^I(t'), j^I(t'')] | \psi(t) \rangle, \quad (8)$$

and in the diamagnetic term, $\tau = t_h \sum_{i,\sigma} (c_{i+1,\sigma}^\dagger c_{i,\sigma} + \text{H.c.})$,

which, different from the current operator in Eq. (4), is the stress tensor operator. The interaction representation of an operator $B^I(t')$ is defined as $U^\dagger(t', t) B U(t', t)$, where $U(t', t)$ is the time-evolution operator *in the absence of probing perturbations*¹⁸. It is clear from the expression that in order to obtain the value of $\sigma(t', t)$, the current-current correlations (commutators) between the intermediate time and the ending time t' have to be taken into account. We call it as NLR.

This seems to be the end of the story. However, from time to time in the literature, we notice that another

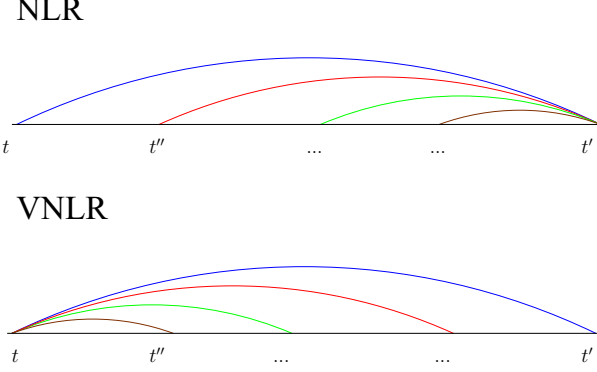


FIG. 1. (Color online) A schematic diagram of the current-current correlations considered in NLR and VNLR, respectively.

kind of generalized Kubo formula in the nonequilibrium (NKF) has been used^{2,16}:

$$\text{Re } \sigma_{\text{reg}}(\omega, t) = \frac{1}{\omega L} \text{Im} \int_0^{t_m} ds \left[ie^{i(\omega+i\eta)s} \times \langle \psi(t) | [j^I(t+s), j^I(t)] | \psi(t) \rangle \right]. \quad (9)$$

A careful analysis shows that the NKF cannot be obtained from the response function in Eq. (7) (with the diamagnetic term dropped) by using the definition of Eq. (6). It seems that another "response function", denoted as $\tilde{\sigma}(t', t)$ ($t' \geq t$) here, is used:

$$\tilde{\sigma}(t', t) = \frac{1}{L} \left[\langle \psi(t') | \tau | \psi(t') \rangle + \int_t^{t'} \chi(t'', t) dt'' \right], \quad (10)$$

where similarly

$$\chi(t'', t) = -i\theta(t'' - t) \langle \psi(t) | [j^I(t''), j^I(t)] | \psi(t) \rangle. \quad (11)$$

We call it VNLR. First it is easy to recognize that NKF in Eq. (9) is just the real regular part of the Fourier transformation of the second term in Eq. (10) with respect to $t' - t$. Further the difference between NLR and VNLR actually comes from the second term in the response functions (Eqs. (7) and (10)), where under the integration over the intermediate moment $t'' \in (t, t')$, the two-time commutators of the current operator take place at t'' to t' , and t to t'' , respectively. Note that t and t' are the starting time and ending time of $\sigma(t', t)$ ($t' \geq t$), respectively. That is to say, different from NLR, $\tilde{\sigma}(t', t)$ instead takes into account the current-current correlations (commutators) between the starting time t and the intermediate time. The above description can be read from Fig. 1.

We argue that the NLR method, which has been derived rigorously from the linear response theory¹⁸, contains more complete information of the temporal correlations than VNLR (or equivalently NKF) *with respect to the definition of $\sigma(\omega, t)$ in Eq. (6)*. The observation

can be easily apprehended from Fig. 1, reminding that $\sigma(\omega, t)$ is the Fourier transformation of $\sigma(t', t)$ with respect to $t' - t$ (with t fixed). The fact suggests that VNLR can be regarded as a kind of partial summation on the temporal correlations of NLR. It should be emphasized that for the equilibrium case, the two produce identical $\sigma(\omega)$ due to the time translation invariance. Then a considerable issue could be raised regarding the validity and limitation of VNLR: in what situation and to what extend can VNLR remain to be a good approximation? Does it impose any specific restriction on the probing fields? In order to address this issue, we now move to our method.

Inspired by the experimental pump-probe setup and the theoretical works on the coherent dynamics in the BCS model^{23,24}, we propose a method to calculate the optical conductivity of the Hubbard model in both equilibrium and out of equilibrium as follows.

First, one notes that an external spatially homogeneous electric field applied along the chain in the Hamiltonian (1) can be incorporated via the Peierls substitution in the hopping terms as²⁵:

$$c_{i,\sigma}^\dagger c_{i+1,\sigma} \rightarrow e^{iA(t)} c_{i,\sigma}^\dagger c_{i+1,\sigma}, \quad H \rightarrow H(t). \quad (12)$$

With the knowledge of the wave function $\psi(t)$ under the action of $A(t)$, the temporal evolution of the expectation value of the current operator $\langle j(t) \rangle$, defined as $\langle j(t) \rangle = \langle \psi(t) | j | \psi(t) \rangle$, can be readily obtained. Note that with the existence of $A(t)$, the current operator j becomes

$$j = \frac{\delta H(t)}{\delta A(t)} = -it_h \sum [e^{iA(t)} c_{i,\sigma}^\dagger c_{i+1,\sigma} - \text{H.c.}] \quad (13)$$

In equilibrium, we set the vector potential $A(t)$ to be a weak probe pulse denoted as $A_{\text{probe}}(t)$, and the current induced by it as $\langle j_{\text{probe}}(t) \rangle$. The optical conductivity can then be calculated by

$$\sigma(\omega) = \frac{j_{\text{probe}}(\omega)/L}{E_{\text{probe}}(\omega)} = \frac{j_{\text{probe}}(\omega)}{i(\omega + i\eta)L A_{\text{probe}}(\omega)}, \quad (14)$$

where $j_{\text{probe}}(\omega)$ and $A_{\text{probe}}(\omega)$ are the Fourier transformations of $\langle j_{\text{probe}}(t) \rangle$ and $A_{\text{probe}}(t)$, respectively. Note that numerically, a damping factor $e^{-\eta t}$ is also introduced when the Fourier transformations are performed, as indicated in Eq. (6). And the same η in the denominator of Eq. (14) is necessary to distinguish the Drude component in the spectral weight at $\omega \rightarrow 0$, which will be discussed later in more detail in Sec. IV.

It is worth to stress here that Eq. (14) can be regarded as a practical definition of the conductivity in equilibrium: $\sigma(\omega)$ does not depend on the details of the probing field we choose, which has been verified in the numerical simulations. We are now in the position to generalize the algorithm to nonequilibrium, where the system, e.g., can be driven either by a pump pulse or a quench. The key is that in order to identify the response of the system with respect to the later probe pulse, a subtraction is necessary, i.e., two successive steps are involved (each step

follows similar process described above) in order to calculate the optical conductivity in nonequilibrium²⁶. First, a time-evolution process in the absence of probe pulse is evaluated and we obtain $\langle j(t) \rangle$. Secondly, in the presence of a additional probe pulse, we get $\langle j_{\text{total}}(t) \rangle$. The subtraction of $\langle j(t) \rangle$ from $\langle j_{\text{total}}(t) \rangle$ produces the required $\langle j_{\text{probe}}(t) \rangle$, i.e., the variation of the current expectations due to the presence of the probe pulse. Then analogous to Eq. (14), the optical conductivity in nonequilibrium is proposed to be

$$\sigma(\omega, t_{\text{probe}}) = \frac{j_{\text{probe}}(\omega, t_{\text{probe}})}{i(\omega + i\eta)LA_{\text{probe}}(\omega)}, \quad (15)$$

where t_{probe} is the probing time. This pump-probe-based method is abbreviated to PP.

A few final words for the numerical method: in order to trace the temporal evolution of the system, we employ the time-dependent Lanczos method to evaluate $|\psi(t)\rangle$. The key formula is

$$|\psi(t + \delta t)\rangle \simeq \sum_{l=1}^M e^{-i\epsilon_l \delta t} |\phi_l\rangle \langle \phi_l | \psi(t) \rangle, \quad (16)$$

where ϵ_l and $|\phi_l\rangle$ are eigenvalues and eigenvectors of the tridiagonal matrix generated in the Lanczos iteration, respectively; M is the dimension of the Lanczos basis and δt is the minimum time step. More details of the algorithm can be found in Ref. 27.

III. THE INFLUENCE OF THE PROBE PULSES - A THEORETICAL ARGUMENT

In the PP method, analogous to experiments, it is important that the strength of the probe pulse should be weak enough to prevent disturbing the system's dynamics qualitatively. Meanwhile, the influence of the forms of the probe pulse is also crucial in nonequilibrium. The point will be made clear in the following arguments.

We begins with the specific form of Eq. (5) in 1D:

$$\langle j_{\text{probe}}(t') \rangle = \int_{t_0}^{t'} \sigma(t', t'') E_{\text{probe}}(t'') dt'', \quad (17)$$

where we have assumed that the probe electric field is turned on after t_0 with the restriction of $t' > t_0$. The Fourier transformation on $\langle j_{\text{probe}}(t') \rangle$ gives

$$\begin{aligned} j_{\text{probe}}(\omega) &= \int_{t_0}^{t_M} \langle j_{\text{probe}}(t') \rangle e^{i\omega t'} dt' \\ &= \int_{t_0}^{t_M} \int_{t_0}^{t'} \sigma(t', t'') E_{\text{probe}}(t'') e^{i\omega t'} dt'' dt' \\ &= \int_{t_0}^{t_M} \left[\int_{t''}^{t_M} \sigma(t', t'') e^{i\omega(t' - t'')} dt' \right] E_{\text{probe}}(t'') e^{i\omega t''} dt'' \\ &= \int_{t_0}^{t_M} \sigma(\omega, t'') E_{\text{probe}}(t'') e^{i\omega t''} dt'', \end{aligned} \quad (18)$$

where t_M is the maximum evolution time and $t_M \gg t_0$. We can see that in order to obtain $\sigma(\omega, t)$ (assuming $t \in (t_0, t_M)$). In this section for notational convenience we use t to denote the probing time), the most convenient choice of E_{probe} in theory is a delta pulse with the form of $E_{\text{probe}}(t'') \sim \delta(t'' - t)$, and the desired $\sigma(\omega, t)$ is simply proportional to $j_{\text{probe}}(\omega)$. The strategy is different from the usual treatment for equilibrium in the textbooks, e.g., in Ref. 28, where a monochromatic perturbation field $E(t) \sim e^{-i\omega t}$ is applied from $t \rightarrow -\infty$. In the temporal gauge, the favorable delta electric field corresponds to a step-like vector potential, i.e., $A_{\text{probe}}(t'') = A_{0,\text{step}} \theta(t'' - t)$, where $\theta(t'')$ is the Heaviside step function (the effect of ramping, i.e., the gradual increase of A_{probe} from zero to a finite value, instead of a jump, will be discussed later in this section). We call this kind of the PP way with a step-like vector potential as PP-step. From Eq. (18) it is easy to convince oneself that under the step potential Eq. (15) exactly produces $\sigma(\omega, t)$ in NLR. It means that by deploying step-like vector potentials at moment t , we can extract the exact value of $\sigma(\omega, t)$ by simply looking at the time evolution of the induced current $\langle j_{\text{probe}}(t) \rangle$. Thus the connection between PP-step and NLR can be established. The proposition will be verified by the later numerical simulations.

However, in the ultrafast spectroscopy measurements, instead of electric delta-like fields, THz AC probe pulses, which usually come from the same source of pump pulses, are employed. It seems that a more realistic approach for a probe pulse could be^{19,29,30}

$$\begin{aligned} A_{\text{probe}}(t'') &= A_{0,\text{probe}} \exp \left[- (t'' - t)^2 / 2t_{d,\text{probe}}^2 \right] \\ &\times \cos [\omega_{\text{probe}} (t'' - t)], \end{aligned} \quad (19)$$

where a Gaussian-like envelope around t is used with $t_{d,\text{probe}}$ characterizing the temporal width of the probe pulse, and ω_{probe} is the central frequency. Following the previous conventions, we call the PP method with the Gaussian-like vector potential as PP-Gaussian. An illustration of Gaussian pulses with different widths t_d is shown in Fig. 2(a).

Let us examine what approximation has to be made in order to justify Eq. (15) in the PP-Gaussian. Suppose that the pulse is activated during $[t, t + \Delta t]$, i.e., $E_{\text{probe}}(t'') \neq 0$ only when $t'' \in [t, t + \Delta t]$, consequently, $\langle j_{\text{probe}}(t') \rangle = 0$ when $t' < t$. From Eq. (18) we have

$$\begin{aligned} j_{\text{probe}}(\omega) &= \int_t^{t+\Delta t} \sigma(\omega, t'') E_{\text{probe}}(t'') e^{i\omega t''} dt'' \\ &\approx \sigma(\omega, t) E_{\text{probe}}(\omega), \end{aligned} \quad (20)$$

which is nothing but Eq. (15). The key approximation lies in the last step of Eq. (20), where $\sigma(\omega, t'')$ is approximately by $\sigma(\omega, t)$. It requires a narrow probe pulse, i.e., $t_{d,\text{probe}}$ should be small enough for nonequilibrium in order to obtain $\sigma(\omega, t)$. It is noted that even in equilibrium, the width of the probe pulse can also influence the

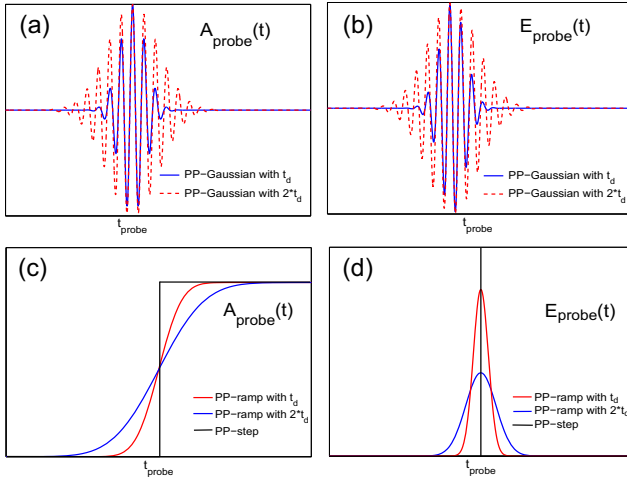


FIG. 2. (Color online) Schematic illustrations of the vector potentials and the corresponding electric fields for the Gaussian pulse ((a), (b)) and step-like pulse ((c), (d)) with various widths.

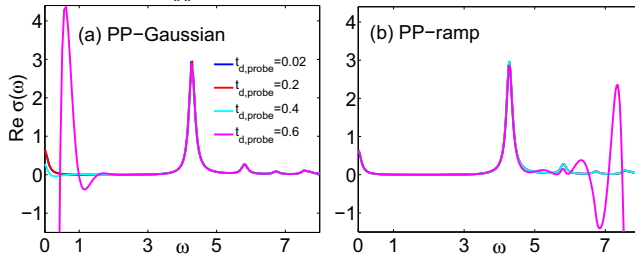


FIG. 3. (Color online) The calculated $\text{Re}\sigma(\omega)$ in equilibrium (zero temperature) for the Hamiltonian (1) with different $t_{d,\text{probe}}$. Parameters: $L = 10$, $U = 10$, $V = 4.5$. (a) By PP-Gaussian with $\omega_{\text{probe}} = 10$, and $A_{0,\text{probe}} = 1.0 \times 10^{-6}$. (b) By PP-ramp with $A_{0,\text{step}} = 1.0 \times 10^{-4}$.

resulting $\sigma(\omega)$, as shown in Fig. 3. In Fig. 3(a), the zero-temperature optical conductivity $\sigma(\omega)$ in equilibrium for the Hamiltonian (1) on the $L = 10$ lattice is calculated by the PP-Gaussian under different values of $t_{d,\text{probe}}$. It shows that when $t_{d,\text{probe}} \leq 0.2$, the results are converged. The reason is following: in PP-Gaussian, the incoming photon frequency is broadened into a Gaussian-like distribution, with the variance of $1/t_d^2$ around ω_{probe} ; in order to cover large enough ω -regime, a sufficiently small $t_{d,\text{probe}}$ is preferred. This observation explains the large deviation for $t_{d,\text{probe}} = 0.6$ at low frequencies when ω_{probe} is set to be 10 in Fig. 3(a).

To make the information complete, we also investigate the ramping effect in PP-step, where a schematic illustration of $A_{\text{probe}}(t)$ with finite increase width (named as PP-ramp) can be found in Fig. 2(b). For the Hamiltonian (1) with identical parameters used in the previous PP-Gaussian calculation, we see that the results converge as $t_{d,\text{probe}} \leq 0.4$, as shown in Fig. 3(b). The noticeable deviation for $t_{d,\text{probe}} = 0.6$ at high frequencies is due to the exponential decay of $A_{\text{probe}}(\omega)$ in the frequency space

with the decay constant proportional to $t_{d,\text{probe}}^2$.

The above discussion tends to suggest that with small enough $t_{d,\text{probe}}$, the results of the PP-Gaussian and PP-step would be the same in general. We have shown that it is actually the case in equilibrium. However there is a critical difference between them. Mathematically, note that in the PP-Gaussian, unlike the PP-step, $A_{\text{probe}}(t'') \rightarrow 0$ as $t'' \rightarrow \pm\infty$, and consequently, the temporal integration over the electric field gives $\int_{t_i}^{t_f} E(t'') dt'' \approx \int_{-\infty}^{+\infty} E(t'') dt'' = 0$, which we believe might also be generally true in experimental situations³¹. The induced current $\langle j_{\text{probe}}(t') \rangle$, as shown in Eq. (17), is produced in the PP-Gaussian by a highly temporally localized perturbation in the range of $[t, t + \Delta t]$ (outside the range, both the electric field and the vector potential are practically zero). It is therefore reasonable to suggest that when the Gaussian-like pulse is used, only the correlations between the variant t' and (roughly) fixed t (probe time) are taken into account in the calculation of $\sigma(\omega, t)$, which coincides with the feature of VNLR when the temporal correlations are concerned (see Fig. 1).

It is instructive to consider a limiting case where we simply put $\omega_{\text{probe}} = 0$, and $t_{d,\text{probe}} \rightarrow 0$, i.e., using a delta-like vector potential. If we put an electric field corresponding to the delta vector potential (a monocycle pulse) into Eq. (5), by using the response function in NLR, after the partial integration, we can find that the resulting $\langle j_{\text{probe}}(t') \rangle$ is proportional to $\chi(t', t)$ (here we just focus on the current-current correlation term). Employing its Fourier transformation into Eq. (15), what we finally obtain is nothing but the expression of NKF in Eq. (10). The loop between PP-Gaussian and VNLR thus can be largely closed. From the above analysis, we propose that the PP-step and PP-Gaussian can be identified with the NLR and VNLR, respectively. The proposition will be examined in the next section numerically.

In the following simulations, we set $t_m \sim 200$, $M = 30$, $\delta t = 0.02$, $\eta = 1/L$, with the lattice size $L = 10$. PP-Gaussian and PP-step (as the limiting case of zero-width PP-ramp) are employed, compared with the results of NLR and VNLR. In the PP-step, $A_{0,\text{step}} = 1.0 \times 10^{-4}$; in the PP-Gaussian, $A_{0,\text{probe}} \sim 10^{-6}$, $t_{d,\text{probe}} = 0.02$, and $\omega_{\text{probe}} = 10$. Only the real parts of the optical conductivity are displayed. Despite double temporal evolutions being involved, the performance of the PP methods can match those of (V)NKF in speed and less memory-demanding because no integration is required¹⁸.

IV. RESULTS AND COMPARISON

In this section, working on the 1D half-filled extended Hubbard model (1), we compare the numerical results of the optical conductivity both in equilibrium and out of equilibrium between various methods.

We first discuss the equilibrium case. Figure 4 shows the results in equilibrium (zero temperature) under the open and periodic boundary conditions (BCs), obtained

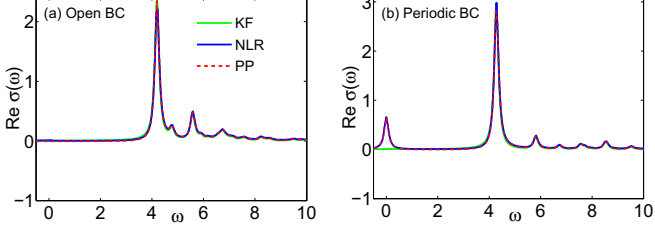


FIG. 4. (Color online) $\text{Re } \sigma(\omega)$ in equilibrium (zero temperature) for the Hamiltonian (1) obtained by the KF, NLR, and PP methods in (a) the open boundary condition (open BC) and (b) periodic BC. Parameters: $L = 10$, $U = 10$, $V = 4.5$.

by KF, NLR and PP. There are no differences between the results of the PP-step and PP-Gaussian. The NKF, as a generalization of KF to nonequilibrium, produces data identical to KF in equilibrium. We can see that the results obtained by the three methods coincide well in the open BC; while in the periodic BC, deviations occur in the vicinity of $\omega = 0$. As shown in Fig. 4(b), an identical peak around zero frequency is produced both by the PP and NLR, while it is absent in the KF result. The small peak is known to originate from the nonzero charge stiffness (Drude weight) in the periodic BC for *finite systems*, even when the system is in an insulating phase. The reason is following. The charge stiffness D is related to the singularity of $\text{Re } \sigma(\omega)$ at $\omega = 0$ as^{32,33}:

$$\text{Re } \sigma(\omega) = 2\pi D\delta(\omega) + \text{Re } \sigma_{\text{reg}}(\omega), \quad (21)$$

and here

$$D = (1/2L)[\langle \tau \rangle + \text{Re } \chi(\omega = 0)], \quad (22)$$

where $\chi(\omega)$ is defined in Eq. (3). We can see that the Drude weight component comes from the net contribution of the diamagnetic term $\langle \tau \rangle$ and the current-current correlations at $\omega = 0$. For an insulator, D might still remain finite especially in the periodic BC when the system size is small, though it should vanish in the thermodynamic limit. It has been confirmed by the sum rule check (not shown here) that for our model at half filling with $L = 10$, D has a sizable value in the periodic BC, while in the open BC the value is negligibly small. The introduction of the η factor in the numerical calculations expands the singularity at $\omega = 0$ into a small peak, as shown in Fig. 4(b). Here we can see that the contribution to the conductivity from the Drude weight can be captured both by the NLR and PP methods, while the KF method, which only takes into account the regular part of the current-current correlations in Eq. (2), fails to produce this feature.

We are ready to move to the nonequilibrium case. As a demonstration, three well-attended situations are considered here. The driving force to nonequilibrium in the first case is a pump pulse with the form similar to Eq. (19) (formally just replace "probe" with "pump"), and we call this situation as Pump case. The second case is to apply

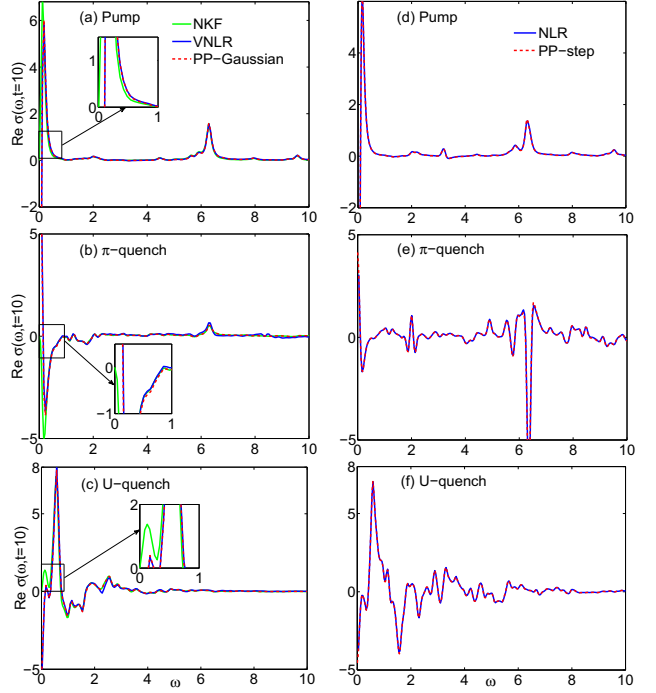


FIG. 5. (Color online) The time-dependent optical conductivity $\text{Re } \sigma(\omega, t)$ at $t = 10$ for the Hamiltonian (1) obtained by different methods in the periodic BC, where t is the time delay between the probe and pump (quench) time. In (a) and (d), a pump pulse is applied with parameters $A_{0,\text{pump}} = 0.2$, $\omega_{\text{pump}} = 6.29$ (resonant frequency), and $t_{d,\text{pump}} = 0.5$. In (b) and (e), a π -quench is applied. In (c) and (f), a U -quench with the U value changed from 10 to 4 is applied. The blue solid lines represent the results of the VNLR in the left column ((a), (b), and (c)) and NLR in the right column ((d), (e), and (f)), respectively, while the red dashed lines represent the results of the PP-Gaussian and PP-step in the two columns. The insets in the left column display the details in the vicinity of $\omega = 0$ obtained by NKF, VNLR and PP-Gaussian. Model parameters: $L = 10$, $U = 10$, $V = 3$.

a temporary delta-like electric pulse, which can be simulated by introducing a phase shift $e^{i\phi\theta(t)}$ in the hopping terms of Eq. (1)²⁵, where $\theta(t)$ is the Heaviside function. The strength of the pulse is controlled by ϕ . In our calculations we choose $\phi = \pi$, an extreme case and known as π -quench. The third case is the U -quench, where a sudden change of U takes place at $t = 0$. This situation can be realized, for example, in cold atoms³⁴.

Figure 5 shows the results of $\text{Re } \sigma(\omega, t)$ at $t = 10$ for these three setups with various methods. First note that the NKF method only includes the regular part of the current-current correlation term (see Eq. (9)). As a result, $\text{Re } \sigma(\omega, t)$ equals to zero at $\omega = 0$ exactly. Away from the vicinity of $\omega = 0$, the results of NKF and VNLR are consistent. This is not surprising since the NKF is just about the regular part of VNLR. More importantly, from Fig. 5, we can see that in all these three cases including pump and quench, the results between PP-Gaussian and VNLR (left column), PP-step and NLR (right col-

umn) coincide well with each other. Thus the proposition in the previous section of the equivalence among these groups is verified numerically. We make it clear that the NKF and NLR, as being widely used in the dynamic response study, actually correspond to different limits of the probe in the PP method, which either has a Gaussian-like vector potential with a vanishing width, or has a step-like one. The former with a tiny width as small as $t_{d,\text{probe}} = 0.02$ actually can be regarded as an approximation of the temporal delta-like potential, which has been numerically confirmed in our calculations (not shown here). Though the electric fields are both highly temporally confined in these two cases, one essential difference is the persistency (or temporal locality in the opposite sense) of the vector potential in the subsequent time evolutions, which results in the (non)vanishing of the time integral of the electric field over the probing time. A possible implication of the above observations is that the time-dependent conductivity or other similar transport quantities in nonequilibrium obtained in experimental measurements, might depend on the details of probe, if the features of the measuring procedures are essentially described by the PP method. Theoretical investigations should take into account the relevant experimental setup sufficiently. In the present THz spectroscopy measurements, the duration time of probe pulses is usually hundreds times larger than the microscopic time unit, which may vindicate the approximation of PP-step or NLR, where the characteristic duration time of probe is much longer than the time scale of the dynamics we are interested in¹⁴. Reversely, i.e., if the probe time scale is much smaller than the later, VNLR or PP-Gaussian might be a good starting point for analysis.

It could be worthwhile to give some supplementary comments on the physics in Fig. 5 before closing the section, though it is not the main subject of the present study. In the Pump case, a prominent Drude-like structure of the transient conductivity at low-frequency regime can be observed, associated with the suppression of the main absorption peak around $\omega = 6.3$. It is a typical phenomenon due to photoinduced carriers. More discussions on this issue in terms of this model can be found, e.g., in Ref. 26. The π -quench corresponds to a population inversion in the kinetic energy³⁵, where a temporally enhancement of charge mobility is also observed. The U -quench is one of the examples of interaction quench²⁰. In our case, with U being switched from 10 to 4, part of the interaction energy is released into the system with the consequent enhancement of the kinetic energy, which also results in the substantial changes of the optical spectrum.

Additionally, as shown in Fig. 5, similar development of $\sigma(\omega, t)$ between the left and right columns can still be recognized regardless of the notable difference in quenches. This is consistent with the previous statement in Sec. II that the VNLR is a kind of partial summation on the full temporal correlations in NLR. In the Pump case, the results of VNLR and NLR are more close to

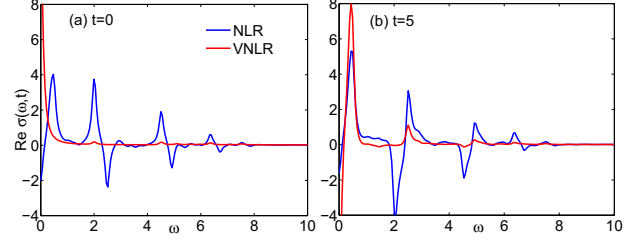


FIG. 6. (Color online) The time-dependent optical conductivity $\text{Re } \sigma(\omega, t)$ for the Hamiltonian (1) obtained by NLR and VNLR in a U -quench case, where U is switched from 0 to 2 at $t = 0$. The probing time is set at $t = 0$ in (a) and $t = 5$ in (b), respectively. Model parameters: $L = 10$, $V = 0$.

each other²⁶ compared with the cases of quenches, which might be due to the fact that, we suspect, the Hamiltonian only changes temporarily by the application of the pump pulse and after that it goes back; while in both π -quench and U -quench, the Hamiltonian undergoes a substantial change after the quench time. Numerical checks in the periodic BC up to $L = 14$ and the open BC in $L = 10$ show similar results. Thus we tend to conclude that the deviation between VNLR and NLR, which is due to different temporal correlation counting, persists with the growing of the system size. Further we note that the deviation of VNLR from NLR can be quite pronounced if the probing time is set to be close to the pump or quench moment before the relaxation fully commences, since different from NLR, VNLR only consider the temporal correlations starting from the probing time t (see Fig. 1). Figure 6 shows $\text{Re } \sigma(\omega, t)$ for the 1D half-filled Hubbard model ($V = 0$ for the Hamiltonian (1)) in a typical U -quench case, where the interaction U is switched from 0 to 2 at $t = 0$. The probing time is set to be $t = 0$ and $t = 5$ in (a) and (b), respectively. Note that at $U = 0$, the ground state of the system is in a metallic state, and with any finite U a charge gap is opened and the system becomes insulating. In Fig. 6(a), we can observe that the resulting $\text{Re } \sigma(\omega, 0)$ from VNLR shows a strong reminiscence of the initial metallic state with a prominent Drude-like peak appearing near zero frequency; while on the other hand, the result from NLR, by taking into account more information of the subsequent nonequilibrium evolution, not only shows the depression of this peak, but also produces additional structures in the higher-frequency regime. However, when the probing time is set at $t = 5$, by then the relaxation between the kinetic energy and the interaction energy is largely finished, the results from VNLR and NLR bear more qualitative similarities.

V. CONCLUSION

In this paper, we introduce a numerical method to calculate the time-dependent optical conductivity based on the simulation of the pump-probe experimental setup.

According to the property of the probe pulse, two different approaches are discussed, i.e., PP-step and PP-Gaussian, using either a step-like or a Gaussian-like probing vector potential. We find that the two approaches can be identified with the nonequilibrium linear response theory and one of its variants, respectively. Thus the connections between these various methods and their differences are clarified. A numerical verification is given by employing the method systematically to the 1D half-filled extended Hubbard model, both in equilibrium and out of equilibrium. The later includes three well-attended cases: the Pump, π -quench and U -quench. In the numerical results, the probe-pulse dependence in nonequilibrium is especially significant in the quenches. We suggest that the nature of the probe pulses should be taken into account in the analysis of ultrafast THz spectroscopy measurements.

ACKNOWLEDGMENTS

The authors thank Janez Bonča, Denis Golež and Dirk Manske for helpful discussions. H.L. acknowledges support from the National Natural Science Foundation of China (NSFC) (Grants Nos. 11325417, 11474136, and 11174115), and the open project of State Key Laboratory of Theoretical Physics (SKLTP) in ITP, CAS. T.T. acknowledges support by the Grant-in-Aid for Scientific Research (26287079) from MEXT and the Strategic Programs for Innovative Research (SPIRE) (hp140215, hp150211), the Computational Materials Science Initiative (CMSI).

* luht@lzu.edu.cn

- ¹ H. Okamoto, H. Matsuzaki, T. Wakabayashi, Y. Takahashi, and T. Hasegawa, *Phys. Rev. Lett.* **98**, 037401 (2007).
- ² S. Wall, D. Brida, S. R. Clark, H. P. Ehrke, D. Jaksch, A. Ardavan, S. Bonora, H. Uemura, Y. Takahashi, T. Hasegawa, *et al.*, *Nature Phys.* **7**, 114 (2011).
- ³ M. Mitrano, G. Cotugno, S. R. Clark, R. Singla, S. Kaiser, J. Stähler, R. Beyer, M. Dressel, L. Baldassarre, D. Nicoletti, A. Perucchi, T. Hasegawa, H. Okamoto, D. Jaksch, and A. Cavalleri, *Phys. Rev. Lett.* **112**, 117801 (2014).
- ⁴ S. Iwai, M. Ono, A. Maeda, H. Matsuzaki, H. Kishida, H. Okamoto, and Y. Tokura, *Phys. Rev. Lett.* **91**, 057401 (2003).
- ⁵ H. Matsuzaki, M. Iwata, T. Miyamoto, T. Terashige, K. Iwano, S. Takaishi, M. Takamura, S. Kumagai, M. Yamashita, R. Takahashi, Y. Wakabayashi, and H. Okamoto, *Phys. Rev. Lett.* **113**, 096403 (2014).
- ⁶ D. Fausti, R. Tobey, N. Dean, S. Kaiser, A. Dienst, M. Hoffmann, S. Pyon, T. Takayama, H. Takagi, and A. Cavalleri, *Science* **331**, 189 (2011).
- ⁷ D. Nicoletti, E. Casandru, Y. Laplace, V. Khanna, C. R. Hunt, S. Kaiser, S. S. Dhesi, G. D. Gu, J. P. Hill, and A. Cavalleri, *Phys. Rev. B* **90**, 100503 (2014).
- ⁸ W. Hu, S. Kaiser, D. Nicoletti, C. Hunt, I. Gierz, M. Hoffmann, M. Le Tacon, T. Loew, B. Keimer, and A. Cavalleri, *Nature Mater.* **13**, 705 (2014).
- ⁹ S. Dal Conte, L. Vidmar, D. Golež, M. Mierzejewski, G. Soavi, S. Peli, F. Banfi, G. Ferrini, R. Comin, B. M. Ludbrook, L. Chauviere, N. D. Zhigadlo, H. Eisaki, M. Greven, S. Lupi, A. Damascelli, D. Brida, M. Capone, J. Bonča, G. Cerullo, and C. Giannetti, *Nature Phys.* **11**, 421 (2015).
- ¹⁰ M. Rini, N. Dean, J. Itatani, Y. Tomioka, Y. Tokura, R. W. Schoenlein, A. Cavalleri, *et al.*, *Nature* **449**, 72 (2007).
- ¹¹ T. Li, A. Patz, L. Mouchliadis, J. Yan, T. A. Lograsso, I. E. Perakis, and J. Wang, *Nature* **496**, 69 (2013).
- ¹² J. Orenstein, *Phys. Today* **65**, 44 (2012).
- ¹³ J. Orenstein and J. S. Dodge, *Phys. Rev. B* **92**, 134507 (2015).
- ¹⁴ D. Nicoletti, M. Mitrano, A. Cantaluppi, and A. Cavalleri, ArXiv e-prints (2015), arXiv:1506.07846 [cond-mat.supr-con].
- ¹⁵ H. Aoki, N. Tsuji, M. Eckstein, M. Kollar, T. Oka, and P. Werner, *Rev. Mod. Phys.* **86**, 779 (2014).
- ¹⁶ G. De Filippis, V. Cataudella, E. A. Nowadnick, T. P. Devoreaux, A. S. Mishchenko, and N. Nagaosa, *Phys. Rev. Lett.* **109**, 176402 (2012).
- ¹⁷ D. Rossini, R. Fazio, V. Giovannetti, and A. Silva, *Europhys. Lett.* **107**, 30002 (2014).
- ¹⁸ Z. Lenarčič, D. Golež, J. Bonča, and P. Prelovšek, *Phys. Rev. B* **89**, 125123 (2014).
- ¹⁹ R. Fukaya, Y. Okimoto, M. Kunitomo, K. Onda, T. Ishikawa, S. Koshihara, H. Hashimoto, S. Ishihara, A. Isayama, H. Yui, and T. Sasagawa, *Nature commun.* **6**, 8519 (2015).
- ²⁰ M. Eckstein, M. Kollar, and P. Werner, *Phys. Rev. B* **81**, 115131 (2010).
- ²¹ M. Eckstein and P. Werner, *Phys. Rev. Lett.* **110**, 126401 (2013).
- ²² R. Kubo, *J. Phys. Soc. Jpn.* **12**, 570 (1957).
- ²³ T. Papenkort, V. M. Axt, and T. Kuhn, *Phys. Rev. B* **76**, 224522 (2007).
- ²⁴ A. P. Schnyder, D. Manske, and A. Avella, *Phys. Rev. B* **84**, 214513 (2011).
- ²⁵ D. Golež, J. Bonča, L. Vidmar, and S. A. Trugman, *Phys. Rev. Lett.* **109**, 236402 (2012).
- ²⁶ H. Lu, C. Shao, J. Bonča, D. Manske, and T. Tohyama, *Phys. Rev. B* **91**, 245117 (2015).
- ²⁷ P. Prelovšek and J. Bonča, in *Strongly Correlated Systems*, Springer Series in Solid-State Sciences, Vol. 176, edited by A. Avella and F. Mancini (Springer, 2013) pp. 1–30.
- ²⁸ G. D. Mahan, *Many-particle physics* (Springer Science & Business Media, 2013).
- ²⁹ H. Lu, S. Sota, H. Matsueda, J. Bonča, and T. Tohyama, *Phys. Rev. Lett.* **109**, 197401 (2012).
- ³⁰ J. Rincón, K. A. Al-Hassanieh, A. E. Feiguin, and E. Dagotto, *Phys. Rev. B* **90**, 155112 (2014).
- ³¹ L. B. Madsen, *Phys. Rev. A* **65**, 053417 (2002).
- ³² H. Castella, X. Zotos, and P. Prelovšek, *Phys. Rev. Lett.* **74**, 972 (1995).
- ³³ X. Zotos and P. Prelovšek, *Phys. Rev. B* **53**, 983 (1996).
- ³⁴ I. Bloch, J. Dalibard, and W. Zwerger, *Rev. Mod. Phys.* **80**, 885 (2008).

³⁵ N. Tsuji, T. Oka, H. Aoki, and P. Werner, Phys. Rev. B **85**, 155124 (2012).